Second harmonic generation in defective hexagonal boron nitride

Renan Cunha[1], Alisson Cadore[1], Sérgio L L M Ramos[2], Kenji Watanabe[3], Takashi Taniguchi[3], Sejeong Kim[4], Alexander S Solntsev[4], Igor Aharonovich[4] and Leandro M Malard[1]

[1] Departamento de Física, Universidade Federal de Minas Gerais, Belo Horizonte, MG 31270-901, Brazil

[2] Centro de Tecnologia em Nanomateriais e Grafeno, Universidade Federal de Minas Gerais, Belo Horizonte, MG 31270-901, Brazil

[3] National Institute for Materials Science (NIMS)—1-2-1 Sengen, Tsukuba-city, Ibaraki 305-0047, Japan

[4] School of Mathematical and Physical Sciences, University of Technology Sydney, Ultimo, New South Wales, 2007, Australia

E-mail: lmalard@fisica.ufmg.br

Abstract

Determining the role of defects in materials can be an important task both for the fundamental understanding of their influence on material properties and for future applications. In this work, we studied the influence of defects on the second harmonic generation (SHG) in hexagonal boron nitride (h-BN). We characterized the sample by photoluminescence imaging and spectroscopy, showing strong and sharp photoluminescence emission at visible range from h-BN flakes due to single defect states. By doing second harmonic imaging, we found strong emission from the h-BN flakes that correlates spatially with the photoluminescence imaging. By doing polarization-resolved SHG, we found deviations from the expected polarization pattern in pristine h-BN samples. We also characterized the nonlinear optical susceptibility of h-BN with defects with a value of one order of magnitude larger than for pristine h-BN, which highlights the role of defects in the efficiency of SHG. Therefore defect engineering could be used as a potential tool for nonlinear optical signal enhancement.

Keywords: 2D materials, nonlinear optics, defects

Since its discovery by Novoselov *et al* [1], graphene has been the focus of intense research [2] due to its novel physical properties [3] and promising technological applications [4]. As a result, the progress in the studies of graphene hampered the discovery of new two-dimensional (2D) materials with new applications and functionalities beyond graphene [5–12]. With the advancement of synthesis and manipulation of the new 2D materials, new applications have come on the scene such as the combination of different 2D materials to form heterostructures [13, 14], and the introduction of defects to modify its physical properties. In the latter case, materials with the ability to host single photon emitter defects have attracted much attention [15–18] due to the importance of single photon emitters for the development of quantum information technologies. A promising candidate arising from this context is hexagonal boron nitride (h-BN) [19–22], a wide bandgap 2D material with several interesting properties [23–26], best known for its use as a dielectric substrate for graphene and

other 2D materials [27, 28]. The midgap defects states in h-BN generate bright and sharp luminescence peaks [29–31] that can be used as single photon sources. In addition to single defect states, h-BN can host different types of defects, such as grain boundaries, edges and stacking disorder. However, the modification of nonlinear optical properties of h-BN due to the presence of different types of defects is still not explored. Here we study how the presence of defects modify the second-order nonlinear optical properties of h-BN.

Because of its honeycomb structure, single layers of h-BN lack inversion symmetry, as opposed to their bulk counterpart. This symmetry breaking gives rise to a finite second-order electric susceptibility ($\chi^{(2)} \neq 0$), which accounts for significant phenomena, such as nonlinear optical effects [32–34]. The properties of second harmonic generation (SHG), a second-order nonlinear process in which two lower energy photons are up-converted into one photon with twice the incident frequency, are already known for pristine h-BN [35, 36]. Additionally, it is also known that the presence of defects can modify the properties of the SHG [37, 38]. Nonetheless, no experimental report has demonstrated the influence of defects on the second-order nonlinear optical properties of h-BN. In this paper, we report modifications on the SHG in h-BN due to the presence of defects, both single defects and structural defects (grain boundaries, edges and stacking disorder, for example). By doing photoluminescence and second harmonic imaging, we find a spatial correspondence between single defects and second harmonic emission. Moreover, by measuring the polarization-dependence and the efficiency of the SHG, we find that the defective samples show deviations from pristine h-BN. By characterizing the second order nonlinear optical susceptibility tensor $\chi^{(2)}$ for the defective h-BN sample, we show that it has a value of one order of magnitude larger than for pristine h-BN.

Photoluminescence (PL) and Raman spectroscopy mapping was done on a Witec alpha300, operating with a 457 nm excitation laser that was focused onto the sample through a 50× objective with a numerical aperture of 0.55. SHG was done in a laser scanning microscope (Lavision Biotec) with a pulsed laser of 180 fs pulse-width and 80 MHz repetition rate, tuned at 810 nm and focused onto the sample with a 40× objective with a numerical aperture of 0.95. The reflected generated second harmonic from the sample was directed through 405/10 nm bandpass filter and detected by a photomultiplier. Additionally, the setup also allows to perform polarization resolved measurements by the introduction of a half-wave plate before the sample and a polarizer at the detector. All measurements were done at room temperature.

The solution of exfoliated h-BN (Graphene Supermarket) was dropcasted in an amorphous quartz substrate and annealed at a temperature of 850 °C under 1 Torr of argon atmosphere. After this thermal treatment the sample was allowed to cool to room-temperature under continuous gas flow. We have selected regions of the sample that contains isolated PL and SHG emission as shown in figure 1 in order to avoid areas with high concentration of h-BN flakes. The number of h-BN layers present in the sample can vary from 1 to 5 according to [39]. Previous works have shown that this type of sample generates different types of single defects in the h-BN structure, leading to bright PL peaks with energy below the h-BN bandgap [19–22]. These defects consist of nitrogen vacancies, boron vacancies, defects formed by the interaction of vacancies with impurities of C, O, H, Ba atoms. Such defects were studied by different experimental techniques and computational modeling in the literature [22, 40–51]. Additional structural defects, such as grain boundaries, edges and stacking faults, are also present in these type of samples [39]. For comparison with the defective sample, a mechanically exfoliated from bulk h-BN sample was used, since the concentration of different types of defects is much smaller.

Figures 1(a) and (c) show the PL intensity images in the 500–700 nm region of the solution exfoliated sample. The two isolated bright spots exhibiting photoluminescence correspond to different regions of the sample. Figure 1(e) presents the PL emission spectrum of each spot, where the lower plot in magenta corresponds to the spot of figure 1(a), while the upper plot in red corresponds to the spot of figure 1(c). As h-BN can not exhibit light emission with such low energy [24], these emissions can therefore be attributed to the presence of single defects produced during the chemical exfoliation and annealing processes. Recently, much attention has been given to such single defects in h-BN, since it has been observed that it constitute stable sources of single photon emitters at room temperature [19–22]. These spectra, together with the others presented in the supplementary material (SM) (stacks.iop.org/JPhysCM/32/19LT01/mmedia), have been previously reported in the literature [19, 22]. Although the identification of defects from PL spectra is still under discussion, *ab initio* calculations propose the association of some of these spectra with certain types of defects as shown in the SM.

Figures 1(b) and (d) shows SHG intensity images of the same area of figures 1(a) and (c). Notwithstanding the differences in the physical origin of each effect, both PL and SHG can be used to map and locate h-BN flakes, showing that the bright spots on one image correspond almost identically to the bright spots on the other. Other images of PL and SHG emissions are shown in the SM. The SHG signal from the h-BN flakes is confirmed by taking the spectra of the emission at 405 nm, which corresponds to half of the incident pump wavelength at 810 nm. Another evidence is that if we tune the laser from 810 to 790 nm, the SHG signal disappears since there is a bandpass filter centered at 405 nm with 10 nm of width only. These results are shown in the SM.

Since h-BN is a non-centrosymmetric material, it generates second harmonic emission [33, 35]. The question here is how the presence of single or other type of structural defects modify the nonlinear optical properties of h-BN. To investigate further the role of different type of defects on SHG, we compared h-BN spots with different emission intensities.

Figure 2 shows images obtained by (a) SHG, (b) Raman scattering and (c) PL of the same two bright spots (green and red arrows). It is possible to see that the most (less) intense spot in the SHG image, identified by the green (red) arrow, does not show the same intensity trend in the Raman and PL

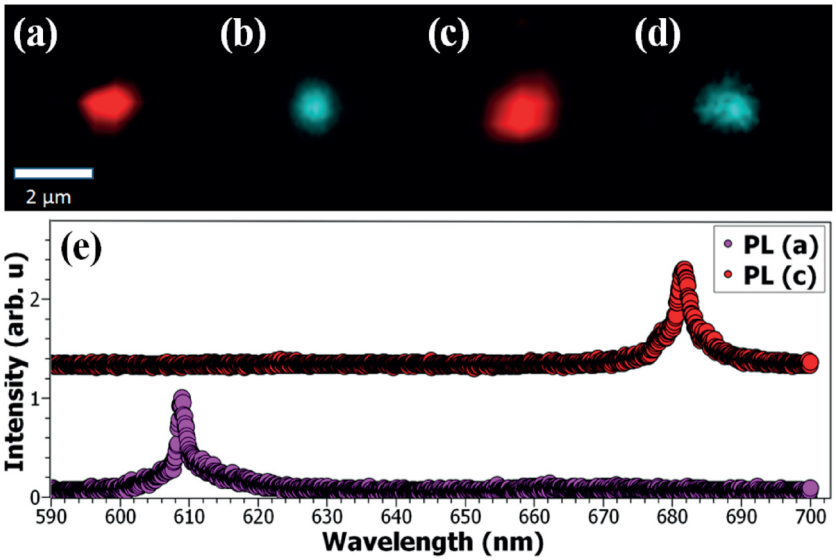

Figure 1. (a) and (c) Photoluminescence intensity image in the region of 500–700 nm. (b) and (d) Show the SHG intensity image of the same regions in (a) and (c) respectively. (e) PL emission spectrum of the spots in (a) (top spectrum) and (c) (bottom spectrum).

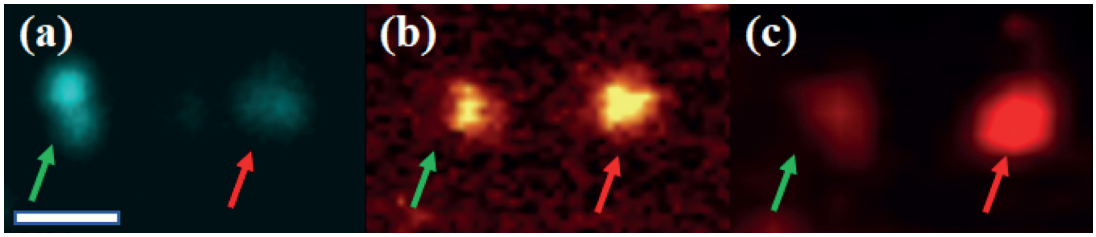

Figure 2. (a) SHG intensity image of two bright spots with distinct intensities (green and red arrows). (b) Raman and (c) photoluminescence (in the 500–700 nm region) intensity images of the same two spots. Scale bar is 2 μm and is the same for all three images.

images. In the case of figure 2(b), it is known that spontaneous Raman scattering scales linearly with material concentration. The comparison of figures 2(a) and (b) suggests that even if the concentration of h-BN contributes to the intensity of SHG, the presence of defects is modifying its emission intensity. In addition to the comparison of figures 2(a) with (b), figure 2(a) alone already carries deviations from expected behaviors for h-BN. It is known that an odd number of layers of h-BN produce SHG with the same intensity as the single layer [35]. This effect is associated with the symmetry of the material and can be explained in terms of the AA' stacking, which provides the necessary conditions for totally destructive interference in even layers [35]. However, figure 2(a) shows two bright spots exhibiting SHG in distinct intensities, evidencing that defects such as stacking faults can be influencing the SHG in h-BN. Another possible mechanism that can explain the distinct SHG, Raman and PL intensities is resonant SHG. Since Raman intensity is density dependent and PL intensity is dependent on the radiative recombination rate of midgaps state from single defects in h-BN, the SHG intensity can be modulated by the resonance of one or two photon absorption with these midgap states. Different h-BN flakes can have different types of single defects [22, 40], which also have different emission energies (figure 1(e) and PL spectra in the SM), and therefore may have different resonances with the SHG. Throughout this sample we have observed h-BN flakes with 5–10 times more second harmonic emission than others. However in our experiments we did not find any correlation between the emitted PL energy and the SHG intensity from different h-BN flakes as shown in the SM.

In order to characterize further the SHG in the defective h-BN samples, we performed polarization-resolved measurements. Figure 3 shows the second harmonic intensity as a function of the incident laser polarization, where the analyzer in front of the detector is kept fixed. In this case, the expected SHG intensity ($I(2\omega)$) dependence with laser polarization (ϕ) is given by $I(2\omega) \propto \sin^2(2\phi)$, revealing a four-fold rotational symmetry [35]. This is expected for samples belonging to point group D_{3h}, which is the case for an odd number of layers of h-BN and other semiconducting transition metal dichalcogenides [52] (More details on SM). Figures 3(a)–(d) shows the SHG intensity angular dependence for four different h-BN flakes. It is possible to observe large deviations from the expected four-fold SHG intensity dependence in pristine h-BN, confirming that the presence of defects is influencing the SHG in h-BN.

Two main mechanisms can explain the polarization behavior (figure 3). The first mechanism follows recent calculations based on group theory that showed that certain defects in h-BN, some of them present in this sample (see SM), belong to

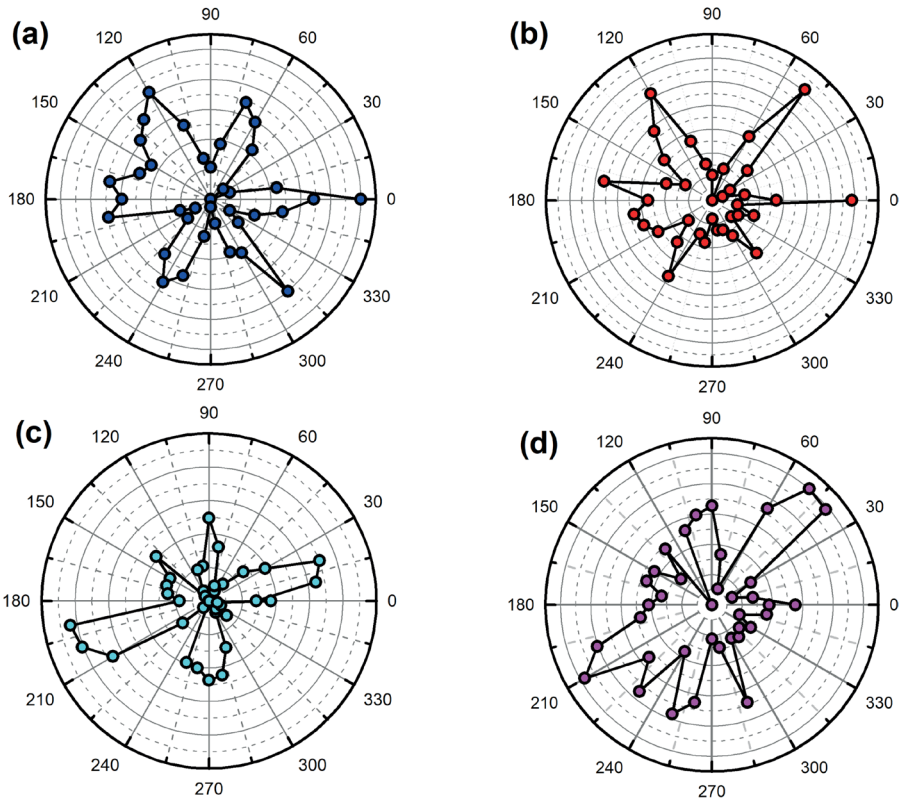

Figure 3. Polar plot of second harmonic intensity from four distinct defective h-BN spots. (a)–(d) Second harmonic intensity as a function of the incident laser polarization is used to show the influence of the defects on the overall second harmonic signal. While a four-fold rotational symmetry is expected for a pristine h-BN sample, the h-BN with defects exhibit a complicated angular dependence.

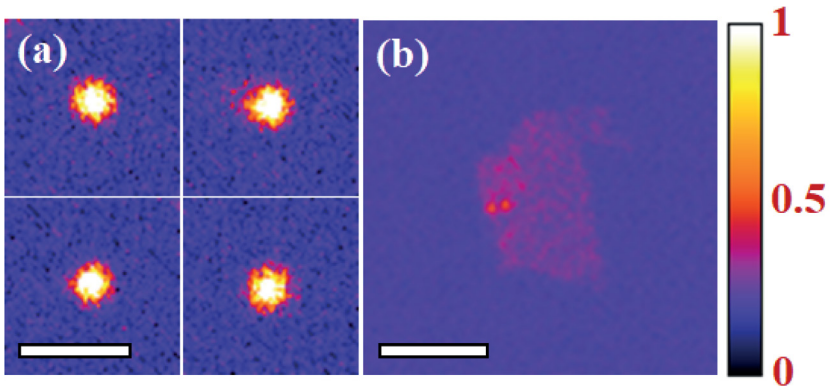

Figure 4. Efficiency of the SHG. SHG intensity image of (a) the defective sample and (b) the mechanically exfoliated sample. Both images were obtained under the same conditions and have the same intensity scale. Scale bars are (a) 2 μm and (b) 5 μm.

point groups that lack inversion symmetry [47, 48]. Therefore, part of the signal can be attributed to a single second harmonic dipole generated by the different single defect states. Also, because of the anisotropic structure of each defect, the dipoles are expected to present different orientations [53]. Contrary to a four-fold emission expected in the absence of defects, we can observe an enhancement of the SHG for some angles due to the overlap with the contribution coming from the defects. In this case, the overall picture of the second harmonic intensity is given by the dependence of a single SH dipole coming from the defect plus the angular dependence of the pristine h-BN [35], giving rise to a complicated SHG angular dependence. The other possible explanation is that the presence of defects changes the condition for totally destructive interference for SHG signal for even number of layers, and therefore different layers contributed to the total SHG signal. In such case the perfect AA' stacking sequence present in bulk h-BN would be disturbed, leading to SHG angular dependence that are not expected for pristine h-BN.

Because of the changes in the characteristics of the SHG emission in h-BN caused by the defects, we turn to the question of efficiency of SHG in this sample. To this end, we measured the second harmonic signal intensity produced by h-BN with defects ($I_{\text{h-BN}}(2\omega)$) and compared with the intensity of a monolayer of MoS_2 ($I_{MoS_2}(2\omega)$). The SHG intensity of both materials were measured with the same experimental conditions, i.e. both samples are on transparent quartz substrates and the parameters for excitation laser and detection was kept

fixed. To evaluate the average intensity of SHG produced by h-BN with defects, we obtained an SHG image of a region of interest and averaged the SHG intensity of different isolated emitting spots as shown in the SM. Finally, we can express the sheet second-order susceptibility of h-BN with defects as:

$$\chi^{*(2)\ s}_{\text{h-BN}} = \frac{\sqrt{I_{\text{h-BN}}(2\omega)}}{\sqrt{I_{MoS_2}(2\omega)}}\chi^{(2)\ s}_{MoS_2}, \quad (1)$$

where $\chi^{(2)\ s}_{MoS_2} = 4.8 \times 10^{-14}$ esu is the second-order susceptibility tensor of a sheet of MoS_2 [35]. With the measured intensities, we find that the sheet second-order susceptibility for the h-BN with defects is $\chi^{*(2)\ s}_{\text{h-BN}} = 3.4 \times 10^{-14}$ esu, which shows a value of about one order of magnitude greater than the measured values for the second-order susceptibility tensor of pristine h-BN which is equal to 1.66×10^{-15} esu [35]. Figure 4 illustrates this result showing that, even visually, the defective h-BN sample in figure 4(a) exhibits SHG with higher intensity compared to an exfoliated high quality h-BN sample shown in figure 4(b).

It is important to note here that we extracted the sheet $\chi^{(2)}$ of h-BN, assuming that few layers are present in the sample [39]. As mentioned above, the AA' stacking may not be present in this case and, therefore, such high value of the sheet $\chi^{(2)}$ can be due to the sum of SHG coming from individual layers. In order to exclude such effects, further measurements with a controlled type of defects would be necessary. However, this is beyond the scope of the present work.

In conclusion, we measured the optical SHG in h-BN with defects. We found a spatial correlation between the SHG and photoluminescence emission from the defect states in h-BN. Polarization measurements of the SHG exhibited deviations from the expected intensity dependence from pristine h-BN samples, which reveals that defects are perturbing the crystal symmetries. Moreover, we characterized the second-order nonlinear susceptibility, which exceeds the typical value of pristine h-BN by one order of magnitude. Further studies are still necessary in order to understand the impact of different types of defects (single defects, grain boudaries, stacking faults) on the second harmonic emission in h-BN. Therefore, controlling the defects responsible for this enhancement can be of great interest in order to enhance the nonlinear optical effects in two-dimensional materials.

Acknowledgments

The authors acknowledge financial support from CNPq, CAPES, FAPEMIG, FINEP and Brazilian Institute of Science and Technology (INCT) in Carbon Nanomaterials and Molecular Medicine.

ORCID iDs

Alisson Cadore https://orcid.org/0000-0003-1081-0915
Kenji Watanabe https://orcid.org/0000-0003-3701-8119
AlexanderSSolntsev https://orcid.org/0000-0003-4981-9730
Igor Aharonovich https://orcid.org/0000-0003-4304-3935
Leandro M Malard https://orcid.org/0000-0003-4207-9653

References

[1] Novoselov K S, Geim A K, Morozov S V, Jiang D, Zhang Y, Dubonos S V, Grigorieva I V and Firsov A A 2004 *Science* **306** 666–9
[2] Novoselov K S *et al* 2012 *Nature* **490** 192
[3] Neto A C, Guinea F, Peres N M, Novoselov K S and Geim A K 2009 *Rev. Mod. Phys.* **81** 109
[4] Jariwala D, Sangwan V K, Lauhon L J, Marks T J and Hersam M C 2013 *Chem. Soc. Rev.* **42** 2824–60
[5] Mounet N *et al* 2018 *Nat. Nanotechnol.* **13** 246
[6] Butler S Z *et al* 2013 *ACS Nano* **7** 2898–926
[7] Mueller T and Malic E 2018 *npj 2D Mater. Appl.* **2** 29
[8] Nicolosi V, Chhowalla M, Kanatzidis M G, Strano M S and Coleman J N 2013 *Science* **340** 1226419
[9] Huang X, Zeng Z and Zhang H 2013 *Chem. Soc. Rev.* **42** 1934–46
[10] Jariwala D, Sangwan V K, Lauhon L J, Marks T J and Hersam M C 2014 *ACS Nano* **8** 1102–20
[11] Chhowalla M, Shin H S, Eda G, Li L J, Loh K P and Zhang H 2013 *Nat. Chem.* **5** 263
[12] Wang Q H, Kalantar-Zadeh K, Kis A, Coleman J N and Strano M S 2012 *Nat. Nanotechnol.* **7** 699
[13] Jariwala D, Marks T J and Hersam M C 2017 *Nat. Mater.* **16** 170
[14] Li M Y, Chen C H, Shi Y and Li L J 2016 *Mater. Today* **19** 322–35
[15] He Y M *et al* 2015 *Nat. Nanotechnol.* **10** 497
[16] Castelletto S, Johnson B, Ivády V, Stavrias N, Umeda T, Gali A and Ohshima T 2014 *Nat. Mater.* **13** 151
[17] Koperski M, Nogajewski K, Arora A, Cherkez V, Mallet P, Veuillen J Y, Marcus J, Kossacki P and Potemski M 2015 *Nat. Nanotechnol.* **10** 503
[18] Doherty M W, Manson N B, Delaney P, Jelezko F, Wrachtrup J and Hollenberg L C 2013 *Phys. Rep.* **528** 1–45
[19] Tran T T, Bray K, Ford M J, Toth M and Aharonovich I 2016 *Nat. Nanotechnol.* **11** 37
[20] Chejanovsky N *et al* 2016 *Nano Lett.* **16** 7037–45
[21] Tran T T, Zachreson C, Berhane A M, Bray K, Sandstrom R G, Li L H, Taniguchi T, Watanabe K, Aharonovich I and Toth M 2016 *Phys. Rev. Appl.* **5** 034005
[22] Tran T T, Elbadawi C, Totonjian D, Lobo C J, Grosso G, Moon H, Englund D R, Ford M J, Aharonovich I and Toth M 2016 *ACS Nano* **10** 7331–8
[23] Edgar J H, Hoffman T B, Clubine B, Currie M, Du X, Lin J and Jiang H 2014 *J. Cryst. Growth* **403** 110–3
[24] Cassabois G, Valvin P and Gil B 2016 *Nat. Photon.* **10** 262
[25] Watanabe K, Taniguchi T and Kanda H 2004 *Nat. Mater.* **3** 404
[26] Weng Q *et al* 2017 *Adv. Mater.* **29** 1700695
[27] Dean C R *et al* 2010 *Nat. Nanotechnol.* **5** 722
[28] Li L H, Santos E J, Xing T, Cappelluti E, Roldán R, Chen Y, Watanabe K and Taniguchi T 2014 *Nano Lett.* **15** 218–23
[29] Katzir A, Suss J, Zunger A and Halperin A 1975 *Phys. Rev.* B **11** 2370
[30] Zunger A and Katzir A 1975 *Phys. Rev.* B **11** 2378
[31] Andrei E, Katzir A and Suss J 1976 *Phys. Rev.* B **13** 2831
[32] Michel K and Verberck B 2009 *Phys. Rev.* B **80** 224301
[33] Boyd R 2008 *Nonlinear Optics* (London: Academic)
[34] Shen Y R 2003 *The Principles of Nonlinear Optics* (New York: Wiley)

[35] Li Y, Rao Y, Mak K F, You Y, Wang S, Dean C R and Heinz T F 2013 *Nano Lett.* **13** 3329–33
[36] Kim S, Fröch J E, Gardner A, Li C, Aharonovich I and Solntsev A S 2019 *Opt. Lett.* **23** 5792–5
[37] Tsai T E, Saifi M A, Friebele E J, Griscom D L and Österberg U 1989 *Opt. Lett.* **14** 1023–5
[38] Saifi M A and Andrejco M J 1998 *Opt. Lett.* **13** 773–5
[39] Coleman J N *et al* 2011 *Science* **331** 568–71
[40] Toledo J R, de Jesus D B, Kianinia M, Leal A S, Fantini C, Cury L A, Sáfar G A M, Aharonovich I and Krambrock K 2018 *Phys. Rev.* B **98** 155203
[41] Geist D and Romelt G 1964 *Z. Nat.forsch.* A **21a** 1970
[42] Museur L, Feldbach E and Kanaev A 2008 *Phys. Rev.* B **78** 155204
[43] Bourrellier R, Meuret S, Tararan A, Stéphan O, Kociak M, Tizei L H G and Zobelli A 2016 *Nano Lett.* **16** 4317–21
[44] Alem N, Erni R, Kisielowski C, Rossell M D, Gannett W and Zettl A 2009 *Phys. Rev.* B **80** 155425
[45] Pennycook S J and Colliex C 2012 *MRS Bulletin* **37** 13–18
[46] Weston L, Wickramaratne D, Mackoit M, Alkauskas A and Van de Walle C G 2018 *Phys. Rev.* B **97** 214104
[47] Abdi M, Chou J P, Gali A and Plenio M B 2018 *ACS Photon.* **5** 1967–76
[48] Sajid A, Reimers J R and Ford M J 2018 *Phys. Rev.* B **97** 064101
[49] Tawfik S A, Ali S, Fronzi M, Kianinia M, Tran T T, Stampfl C, Aharonovich I, Toth M and Ford M J 2017 *Nanoscale* **9** 13575–82
[50] Shevitski B *et al* 2019 *Phys. Rev.* B **100** 155419
[51] Ruoff R 2008 *Nat. Nanotechnol.* **3** 10–1
[52] Malard L M, Alencar T V, Barboza A P M, Mak K F and De Paula A M 2013 *Phys. Rev.* B **87** 201401
[53] Koperski M, Nogajewski K and Potemski M 2018 *Opt. Commun.* **411** 158–65